

INTEGRATION OF CGPS AND GROUND METEOROLOGICAL OBSERVATIONS FOR MITIGATING ATMOSPHERIC EFFECTS ON INSAR

Z.W. LI, X.L. DING, Y.Q. CHEN, Z.L. LI, G.X. LIU

Department of Land Surveying and Geo-Informatics, Hong Kong Polytechnic University
Hung Hom, Kowloon, Hong Kong, China
(zhiwei.li, lsxlding, lsyqchen, lszlli, gx.liu)@polyu.edu.hk

Commission II, WG II /2

KEY WORDS: CGPS, InSAR, Zenith Delay, Atmospheric Effects, Meteorological Data

ABSTRACT:

Repeat-pass interferometric synthetic aperture radar (InSAR) has been demonstrated useful for topographic mapping and surface deformation measurement. However, the interferometric phases of satellite radar signals are often seriously contaminated by atmospheric effects. Due to the highly variable nature of the atmosphere, especially the atmospheric water vapor, it is usually difficult to accurately model and correct the atmospheric effects. Consequently, significant errors are often resulted in InSAR measurements, especially in tropical regions like Hong Kong (HK).

This paper studies a method for mitigating atmospheric effects on InSAR measurements based on an integrated use of Continuous GPS (CGPS) and ground meteorological observations. The tropospheric zenith delays (ZNDs) at a number of CGPS and ground meteorological stations in HK are first estimated and then used to construct a ZND map with a modified Kriging interpolator. Cross-validation tests show that the mean value of the interpolation residuals is close to 0 and the RMS error is about 0.6 cm. When assuming a Gaussian distribution and under 95% confidence level, the interpolation errors are in range of -1.267 cm and 1.269 cm.

The study shows that the temporal and spatial variations of the tropospheric ZNDs can potentially cause a peak-to-peak error in a SAR interferogram of about 9.36 cm at the 95% confidence level for a one-day interval. The error increases to about 11.47cm for a ten-day interval. When the interpolation results are applied to correct the atmospheric effects, the peak-to-peak errors are reduced to 7.50 cm and 9.19 cm respectively for the one-day and ten-day intervals. This shows a 20% reduction in the peak-to-peak errors.

1. INTRODUCTION

Interferometric synthetic aperture radar (InSAR) has been applied widely in recent years for topographic mapping and ground displacement monitoring. The all-weather, day and night imaging capabilities, and the unprecedented spatial coverage and resolution make the technology unique for many types of applications. InSAR has however its shortcomings. One of the most intractable problems is the effect of the atmosphere, especially the atmospheric water vapor, on repeat-pass InSAR measurements. Past studies have shown that spatial and temporal changes of 20% in the relative humidity of the atmosphere could lead to 10 to 14 cm errors in the deformation measurements and to 80 to 290 m errors in the derived terrain models for baselines between 400 m and 100 m in the case of the SIR-C/X-SAR (Zebker et al., 1997). The atmospheric effect is therefore a limiting factor for repeat-pass InSAR applications (Massonnet and Feijl, 1995; Rosen et al., 1996; Tarayre et al., 1996). The effects can be especially significant in humid regions like Hong Kong (HK).

Several approaches have been proposed for atmospheric effect mitigation in InSAR measurements. They can however be summarized as (1) selecting SAR image pairs obtained under favorable weather conditions, (2) averaging SAR interferograms and (3) calibration with external data sources (Hanssen, 1998; Zebker et al., 1997; Delacourt et al., 1998; Williams et al., 1998; Ferretti et al., 1999). For the first two methods, some images apparently cannot be used. Besides, averaging interferograms will degrade the temporal resolution of the measurement results. This is not desirable for areas that continuously deform. As for method 3, the main problem is the usually limited spatial

resolution of external data. Bock and Williams (1997) and Williams et al. (1998) consider using measurements of continuous GPS network to reduce atmospheric noise in InSAR measurements. Delacourt et al. (1998) present a case study of correcting atmospheric errors by using meteorological observations at a reference point together with models of the vertical gradient of the meteorological parameters and of the tropospheric delays. Only long-wavelength components of the atmospheric noise can usually be removed with these approaches due to the sparsity of the meteorological data available.

We will study to integrate CGPS and ground meteorological observations to model and correct the atmospheric effects on InSAR measurements, and to use HK as a test bed for the study. The paper will first provide some general background on atmospheric effects on repeat-pass InSAR. The methods for integrating the two data sources to model and correct atmospheric effects will then be discussed. The effectiveness of the proposed method will finally be discussed.

2. ATMOSPHERE EFFECTS ON REPEAT-PASS INSAR

Of all the atmospheric layers, the ionosphere and the troposphere are the main ones degrading the quality of InSAR measurements. The ionosphere is a frequency-dispersive medium (Rosen et al., 1999; Hanssen, 1998) while the troposphere is not. The troposphere contains about 80% of the total molecular mass of the atmosphere and nearly all the water

vapor. The water vapor is a highly variable component in the troposphere and is responsible for most of the atmospheric errors in InSAR measurements.

When the microwave propagates through the atmosphere, it can be both bent and delayed. The propagation delay dominates in InSAR measurements (Rosen et al. 1999). When considering the propagation delays, the phase measurements of the repeat-pass InSAR can be written as:

$$\psi_1 = \frac{4\pi}{\lambda}(\rho_1 + \Delta\rho_1), \quad \psi_2 = \frac{4\pi}{\lambda}(\rho_2 + \Delta\rho_2) \quad (1)$$

where ρ_1 and ρ_2 are the slant ranges between a ground resolution cell and the SAR platform; λ is the radar wavelength; and $\Delta\rho_1$ and $\Delta\rho_2$ are the propagation delays of the first and the second image acquisitions.

This gives the interferometric phase

$$\phi = \psi_1 - \psi_2 = \frac{4\pi}{\lambda}(\rho_1 - \rho_2) + \frac{4\pi}{\lambda}(\Delta\rho_1 - \Delta\rho_2) \quad (2)$$

where $\frac{4\pi}{\lambda}(\rho_1 - \rho_2)$ is the interferometric phase induced by

the topography and surface deformation, and $\frac{4\pi}{\lambda}(\Delta\rho_1 - \Delta\rho_2)$ is the interferometric phase induced by the atmospheric delays, which can be cancelled out if the atmospheric profile remains the same between the two acquisitions. Besides, the atmospheric effects can also be cancelled out if the interferometric phase caused by the atmosphere is the same for all the resolution cells in an area of interest. Therefore, it is the temporal and spatial non-uniformity of the atmosphere that causes the errors in InSAR measurements. The atmospheric signatures are easily mixed with or misinterpreted as the topographic or ground deformation signals or noise (Hanssen, 1998; Hanssen et al., 1999).

3. ZNDs ESTIMATION FROM CGPS AND METEOROLOGICAL OBSERVATIONS

3.1 ZNDs Estimation from CGPS Observations

Tropospheric ZNDs at CGPS stations can be estimated along with other geodetic parameters (e.g., Bevis et al., 1992). The accuracy of GPS ZND measurements is generally higher than 10 mm. Since the troposphere is a non-dispersive medium, we can use the ZNDs estimated from CGPS to correct InSAR data after they are converted to the radar line-of-sight (LOS) direction.

There are currently six GPS tracking stations in operation in HK located at Fanling, Kam Tin, Kau Yi Chau, Lam Tei, Siu Lang Shui, and Shatin (Figure 1). Seven more stations are under construction. In this study, GPS data received at the six stations from March 1st to March 31st, 2001 are used to estimate the hourly ZNDs together with the other geodetic parameters. Due to some data recording problems, the hourly ZNDs on March 27th 2001 could not be used for all the stations, either could

those on March 20th, 21st and 22nd 2001 for Siu Lang Shui and on March 6th 2001 for Kau Yi Chau. The estimated ZNDs for the six stations are shown in Figure 2.

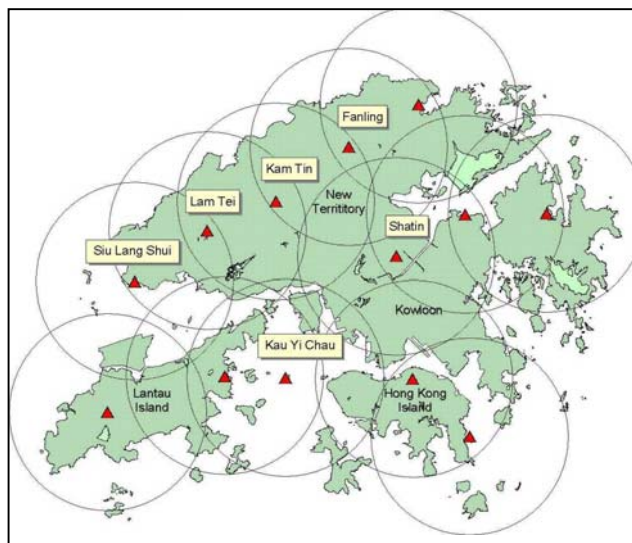


Figure 1. Locations of the six GPS tracking stations (those with names labelled). The other 7 stations are currently under construction (Kwok, 2002).

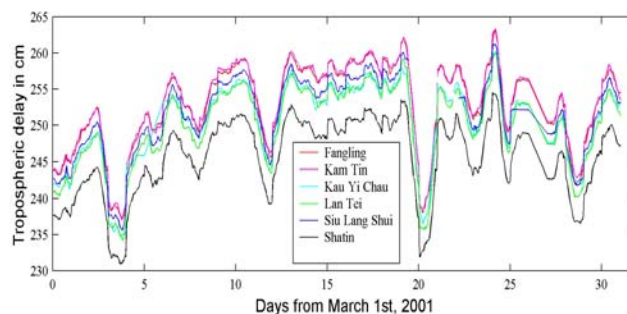


Figure 2. Hourly tropospheric ZNDs at six GPS tracking stations.

3.2 ZNDs Estimation from Ground Meteorological Data

There are in HK 27 evenly distributed automatic meteorological stations operated by the Hong Kong Observatory (HKO). At each of the automatic meteorological stations, measurements of atmospheric pressure, temperature, relative humidity, winds, etc., are normally recorded automatically every minute (HKO, 1999). Tropospheric ZNDs can be estimated from the ground meteorological data. There are numerous empirical models for this purpose, e.g., Hopfield (1971), Saastamoinen (1972), Askne and Hordius (1987), and Baby et al. (1988).

There is also in HK a radiosonde station located at King's Park. The radiosonde ascents to measure upper winds, pressure, temperature and relative humidity at Hong Kong local time 8:00 and 20:00 (HKO, 1999). The recorded profiles of atmospheric pressure, temperature, and relative humidity allow an accurate estimation of vertical refractivity profiles and thus an accurate estimation of the ZNDs at the station.

In order to assess which empirical tropospheric model works best for this region, the data from the radiosonde station are used to evaluate the four commonly used empirical tropospheric models mentioned above. The results obtained based on the data for Jan. 1st, 2000 to Aug. 31st, 2001 are given in Table 1.

Item	Hopfield	Saastamoinen	Askne's	Baby's
offset(cm)	0.5	4.0	1.9	0.4
RMS(cm)	4.3	5.9	4.7	4.2

Table 1. Evaluation results of four empirical tropospheric models

It can be seen from the results that the Hopfield model and the Baby's semi-empirical model work better than the other two models. Baby's semi-empirical model will thus be used for this study. The ZNDs for 9 of the 27 meteorological stations are calculated with the model as the other stations did not record all temperature, pressure and humidity data in March, 2001 or they are far from the northwest part of HK where the CGPS stations located. The results for four of the stations, King's Park, HK Observatory, HK New Airport and Shek Kong are given in Figure 3 as example.

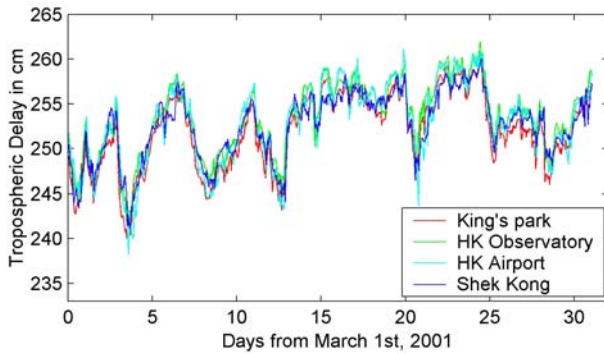


Figure 3. Tropospheric ZNDs at four ground meteorological stations

4. INTEGRATION OF CGPS AND METEOROLOGICAL MEASUREMENTS

Atmospheric disturbances can occur on very small spatial scales, i.e., 100m or shorter (Zebker et al, 1997). This makes it difficult to model and mitigate the atmospheric effects on InSAR since the resolution of external meteorological data sources are usually much lower. The atmospheric disturbances however follow approximately the $-8/3$ power law and on average, 90% of the disturbance energy has wavelengths longer than 400m (Goldstein, 1995; Hanssen, 1998; Williams et al., 1998; Ferretti et al., 1999). The power law nature of the atmospheric disturbances implies that the lower a frequency is, the more energy it accounts for.

We first estimate the tropospheric ZNDs for the CGPS and the meteorological stations in HK as discussed above and then integrate the results to form a ZND map of the area of interest. The Kriging interpolator (Williams et al., 1998; Pham, 2000) is used to interpolate the data. When assuming that there are n sampled locations and m unsampled locations, the weight set

$\{w_1, w_2 \dots w_n\}$ for the p th unsampled location satisfies the following equations

$$\begin{cases} \sum_{j=1}^n w_j \sigma_{ij} + \lambda = \sigma_{ip}, i = 1, \dots, n \\ \sum_j w_j = 1 \end{cases} \quad (3)$$

where σ_{ij} is the covariance of the atmospheric delays at location i and location j ; σ_{ip} is the covariance of atmospheric delays at location i and unknown location p ; and λ is the Lagrange multiplier. Equation (3) above represents a linear equation group and can be resolved by direct matrix inversion (Pham, 2000).

The covariance σ_{ij} can be calculated according to (Schultz et al., 1999):

$$\sigma_{ij} = \sigma_i \cdot \sigma_j \cdot \rho_{ij} \quad (4)$$

In our computations, the sampled values, i.e., the ZND measurements from the CGPS and the meteorological observations have different accuracy. The values we have adopted are $\sigma_i = 1$ cm for the ZNDs at the GPS stations and $\sigma_i = 4.2$ cm for those at the ground meteorological stations. The latter is determined based on the results given in Table 1, the RMS of the Baby's semi-empirical model.

The correlation function ρ_{ij} can be calculated based on the theoretical variance-covariance function of the atmospheric fluctuations (Williams et al. 1998),

$$\rho_{ij} = \frac{Cov(i, j)}{\sqrt{Cov(i, i) \cdot Cov(j, j)}} = \frac{D_\tau(\infty) - D_\tau(R)}{D_\tau(\infty)} \quad (5)$$

where $D_\tau(x)$ is the structure function of the tropospheric delay fluctuations and R is the temporal and spatial distance between point i and j .

The calculated ZNDs for the two SAR acquisitions can be used to correct the SAR interferogram. We will perform a cross-validation test to examine the accuracy of the ZND map thus obtained. Each of the six CGPS points will be removed in turn from the data set when constructing the ZND model and the ZND difference between the modeled and the GPS derived values for each of the points is calculated. The ZND differences thus calculated are called interpolation residuals here for simplicity and are given in Figure 4. Some statistics of the results are given in Table 2.

We can see from Table 2 that the mean values of the interpolation residuals are close to 0 and the RMS values are less than 1 cm for all the CGPS stations. When assuming Gaussian distribution, the overall interpolation precision is between -1.267 cm and 1.269 cm under 95% confidence level.

Station	Max	Min	Mean	RMS
Fanling	1.389	-2.154	-0.002	0.678
Kam Tin	1.305	-1.473	0.002	0.504
Kau Yi Chau	2.553	-2.685	0.003	0.760
Lam Tei	1.006	-1.056	0.001	0.367
Siu Lang Shui	1.920	-3.019	-0.001	0.694
Shatin	1.978	-2.250	0.002	0.712
All six stations	2.553	-3.019	0.001	0.634

Table 2. Statistics of the interpolation residuals (unit: cm)

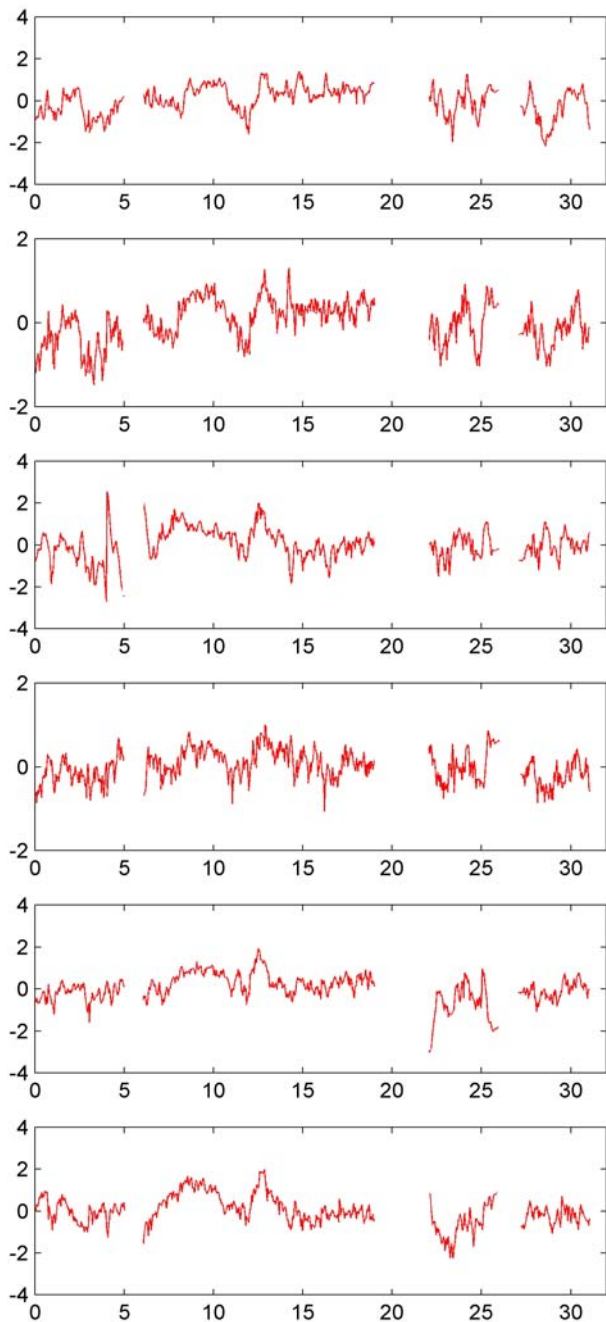


Figure 4. Interpolation residuals at the six GPS stations, Fanling, Kam Tin, Kau Yi Chau, Lam Tei, Siu Lang Shui, and Shatin (from top down) (in cm). The abscissa are number of days starting from March 1st, 2001. The discontinuities in the plots are due to data gaps.

5. COMPARISON AND DISCUSSIONS

Since it is the differential atmospheric delays that affect the InSAR measurements (e.g., Rosen et al., 1996), we will look more closely at the differentiated ZNDs. The hourly ZNDs at each station are first differentiated with a time interval of one day and then ten days. The results are then differentiated again between the stations. The histograms of the double differentiated ZNDs are given in Figure 5 (one-day interval) and Figure 6 (ten-day interval), respectively. A summary of the statistics is given in Table 3.

Intervals	Max	Min	Max-Min	Mean	RMS
1 day	6.37	-5.18	11.55	0.016	1.077
10 days	6.12	-5.99	12.11	0.152	1.320

Table 3. Statistics of double differentiated ZNDs (unit: cm)

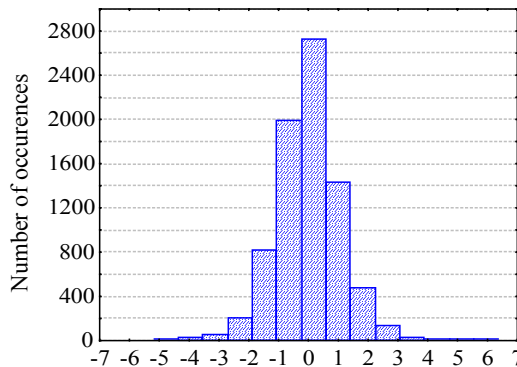


Figure 5. Histogram of double differentiated ZNDs (one-day interval).

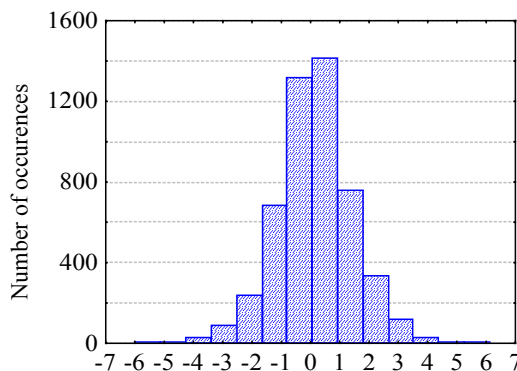


Figure 6. Histogram of double differentiated ZNDs (ten-day interval).

Although the peak-to-peak variability of the double differentiated ZNDs reaches 11.55 cm and 12.11 cm respectively for the one-day and ten-day intervals, Figures 4 and 5 show that the probability for such large values to occur is low. Under the assumption of Gaussian distribution, the double differentiated ZNDs for the one-day interval range from -2.14 cm to 2.17 cm at the 95% significance level. The corresponding values for the ten-day interval are -2.49 cm and 2.79 cm, respectively. Therefore the peak-to-peak variability of the results is 4.31 cm and 5.28 cm, respectively. When assuming a

look angle of 23° (the look angle of the mid scene of the ERS-1/2 images), the ZNDs are translated into 9.36 cm and 11.47 cm of round trip radar signal delays. This level of tropospheric delays can make cm-level ground displacements unobservable and can introduce height errors as large as 320 m and 390 m for a perpendicular baseline of 100m.

To check the effectiveness of the method for mitigating the atmospheric effects on InSAR measurements, we first calculate the interpolation residuals and then estimate how much errors the residuals can introduce in a SAR interferogram. For the latter part, the interpolation residuals are also differentiated twice, first between time points (one-day and ten-day intervals respectively) and then between stations. The histograms of the double differentiated interpolation residuals for the one-day and the ten-day intervals respectively are plotted in Figures 7 and 8. Table 4 gives the associated statistics.

Interval	Max	Min	Max-Min	Mean	RMS
1 day	5.69	-4.45	10.14	0.003	0.863
10 days	4.67	-4.80	9.47	0.133	1.058

Table 4. Statistics of double differentiated interpolation residuals (in cm)

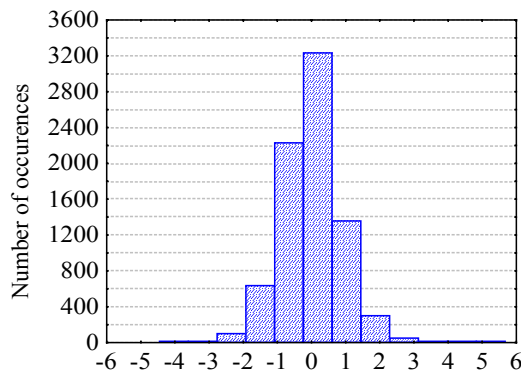


Figure 7. Histogram of double differentiated interpolation residues (one-day interval).

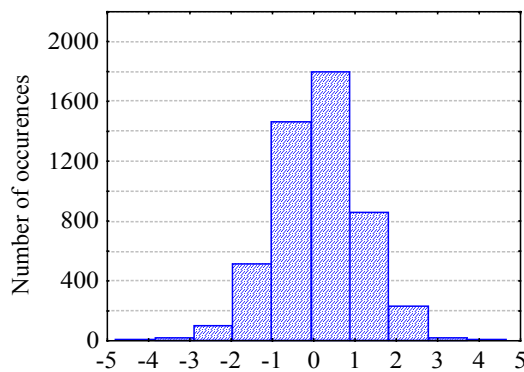


Figure 8. Histogram of double differentiated interpolation residuals (ten-day interval).

Assuming again Gaussian distribution and 95% confidence level, the peak-to-peak variabilities for the one-day and ten-day

intervals are 3.45 cm and 4.23 cm, respectively, which amount to 7.50 cm and 9.19 cm when mapped to two-way radar path delays. This shows improvements of 19.87% and 19.89% when compared with the uncorrected results. It can be expected that the improvements will be more significant with if CGPS stations and meteorological stations are available in the area.

6. CONCLUSIONS

A method to mitigate atmospheric effects on InSAR measurements by integrating CGPS and ground meteorological observations has been studied with data from the HK region. The tropospheric ZNDs at the CGPS and the ground meteorological stations were first estimated. A ZND map for the studied area was then formed by interpolating the data with a modified Kriging interpolator. Cross-validation tests have shown that the mean value of the interpolation residuals is close to 0 and the RMS value is 0.634 cm (See Table 2). Assuming a Gaussian distribution, the interpolation errors are in the range of -1.267 cm to 1.269 cm under 95% confidence level.

When no correction is made to the SAR data, the temporal and spatial variations of the tropospheric ZNDs can potentially cause a peak-to-peak error of about 9.36 cm and 11.47 cm in a SAR interferogram at the 95% confidence level for the one-day and ten-day intervals respectively. When the mitigation method is implemented, the peak-to-peak errors are reduced to 7.50 cm and 9.19 cm, respectively. This shows improvements of 19.87% and 19.89%, respectively for the two time intervals, in the accuracy of the interferogram. The accuracy should be further improved if more GPS stations and automatic meteorological stations are available.

ACKNOWLEDGEMENTS

The first author is grateful to the Hong Kong Polytechnic university for the Postgraduate Research Scholarship provided. We thank Dr. Yanxiong Liu for his help in processing the GPS data and for useful discussions.

REFERENCES

- Askne, J. and Nordius, H., 1987. Estimation of tropospheric delay for microwaves from surface weather data. *Radio Science*, 22(3), pp.379-386.
- Baby, H.B., Gole, P., and Lavergnat, J., 1988. A model for the tropospheric excess path length of radio waves from surface meteorological measurements. *Radio Science*, 23(6), pp.1023-1038.
- Bevis, M., Businger, S., Herring, T.A., Rocken, R., Anthes, R.A., and Ware, R.H., 1992. GPS Meteorology: Remote sensing of atmospheric water vapor using the Global Positioning System. *Journal of Geophysical Research*, 97(D14), pp.15787-15801.
- Bock, Y. and Williams, S., 1997. Integrated Satellite Interferometry in Southern California. *EOS*, 78(29), pp.293, 299-300.
- Delacourt, C., Briole, P., Achache, J., 1998. Tropospheric corrections of SAR interferograms with strong topography: application to Etna. *Geophysical Research Letter*, 25(15), pp.2849-2852.

- Ferretti, A., Prati, C. and Rocca, F., 1999. Multibaseline InSAR DEM Reconstruction: The Wavelet Approach. *IEEE Transactions on Geoscience and Remote Sensing*, 37(2), pp.705-715.
- Goldstein, R., 1995. Atmospheric limitations to repeat-track radar interferometry. *Geophysical Research Letter*, 22(18), pp.2517-2520.
- Hanssen, R.F., 1998. Atmospheric heterogeneities in ERS tandem SAR interferometry. DEOS Report No.98.1, Delft University press, Delft, the Netherlands.
- Hanssen, R.F., Wechwerth, T.M., Zebker, H.A., and Klees, R., 1999. High-resolution water vapor mapping from interferometric radar measurements. *Science*, 283, pp.1295-1297
- HKO, 1999. Summary of Meteorological Observations in Hong Kong. Hong Kong Observatory, pp.83.
- Hopfield, H.S., 1971. Tropospheric effect on electron-magnetically measured range: Prediction from surface weather data. *Radio Science*, 6(3), pp.357-367.
- Kwok, S., 2002. Personal communications.
- Massonnet, D., and Feigl, K. L., 1995. Discrimination of geophysical phenomena in satellite radar interferograms. *Geophysical research letters*, 22(12), pp.1537-1540.
- Pham, T. D., 2000. Image restoration by ordinary kriging with convexity. In: *proceedings of the 15th international conference on pattern recognition*, 3, pp.330-333.
- Rosen, P.A., Hensley, S., Zebker, H.A. and et al., 1996. Surface deformation and coherence measurements of Kilauea Volcano, Hawaii, from SIR-C radar interferometry. *Journal of Geophysical Research*, 101(E10), pp.23109-23125.
- Rosen, P.A., Hensley, S., Joughin, I.R. and et al., 1999. Synthetic Aperture Radar Interferometry. In: *Proceedings of The IEEE*, Vol. XX, No. Y.
- Saastamoinen, J., 1972. Atmospheric correction for troposphere and stratosphere in radio ranging of satellites. *The use of artificial satellites for Geodesy*, Geophys. Monogr. Ser., pp.247-251.
- Schultz, C.A., Myers, S.C., Hipp, J. and Yong, C.J., 1999. Nonstationary Bayesian kriging: a predictive technique to generate spatial corrections for seismic detection, location and identification. *Physics of the Earth and Planetary Interiors*, 113(1-4), pp.321-338.
- Tarayre, H. and Massonnet, D., 1996. Atmospheric propagation heterogeneities revealed by ERS-1. *Geophysical Research letters*, 23(9), pp.989-992
- Williams, S., Bock, Y., and Fang, P., 1998. Integrated satellite interferometry: Tropospheric noise, GPS estimates and implications for interferometric synthetic aperture radar product. *Journal of geophysical research*, 103(B11), pp.27051-27067.
- Zebker, H. A., Rosen, P. A. and Hensley, S., 1997. Atmospheric effects in interferometric synthetic aperture radar surface deformation and topographic maps. *Journal of Geophysical Research*, 102(B4), pp.7547-7563.